npj Flexible Electronics

https://doi.org/10.1038/s41528-026-00556-2

Article in Press

Highly robust ECG electrodes constructed from semi-liquid metal fibers for reliable emergency rescue monitoring

Received: 27 October 2025

Accepted: 17 February 2026

Cite this article as: Liu, X., Xu, H., Chen, L. *et al.* Highly robust ECG electrodes constructed from semi-liquid metal fibers for reliable emergency rescue monitoring. *npj Flex Electron* (2026). https://doi.org/10.1038/s41528-026-00556-2

Xiaotong Liu, Hui Xu, Linglong Chen, Xin Lyu, Xiaoshuai Wang, Yanqing Liu, Haojun Fan & Rui Guo

Highly robust ECG electrodes constructed from semi-liquid metal fibers for reliable emergency rescue monitoring

Xiaotong Liu[1†], Hui Xu[1†], Linglong Chen[1,2], Xin Lyu[3], Xiaoshuai Wang[4], Yanqing Liu[1,3]*, Haojun Fan[1,3]*, Rui Guo[1,4]*

1 School of Disaster and Emergency Medicine, Tianjin University, Tianjin, 300072, China.

2 Emergency Medicine Department, Wenzhou Peoples' hospital, The Wenzhou Third Clinical Institute Affiliated to Wenzhou Medical University, Wenzhou, 325000, China.

3 Emergency Department, The First Affiliated Hospital of Wenzhou Medical University, Wenzhou, 325000, China.

4 State Key Laboratory of Cryogenic Science and Technology, Technical Institute of Physics and Chemistry, Chinese Academy of Sciences, Beijing, 100190, China.

†These authors contributed equally to this work.

*Corresponding author: Y. L. (lyq13920406163@tju.edu.cn), H. F. (fanhj@tju.edu.cn), R. G. (guorui@mail.ipc.ac.cn)

Abstract

Global disasters are occurring with increasing frequency, and the stable acquisition of physiological electrical signals from injured individuals is crucial in emergency rescue operations. Conventional patch electrodes are susceptible to signal distortion due to skin contamination and body movement, and their poor breathability often causes discomfort, making them inadequate for rescue scenarios. This study proposes a highly robust surface electrode based on semi-liquid metal (SLM) fibers. The electrode employs pre-stretched elastic fibers as the substrate, coated with SLM to achieve high electrical conductivity, and utilizes wrapping-induced constriction force to enhance fixation. The SLM fiber electrode is not affected by skin contaminants and can be tightly wrapped around multiple limb parts. The wrapped structure of the fiber electrode provides high breathability, preventing skin irritation, and allows rapid and efficient deployment. In practical applications, this SLM fiber electrode facilitates the reliable acquisition of electrocardiogram (ECG) signals, enabling the monitoring in emergency situations as well as continuous and comfortable ECG monitoring after surgery, and provides an innovative solution for emergency medical monitoring.

Introduction

Against the backdrop of frequent global natural disasters and increasing anthropogenic accidents, the acquisition of physiological electrical signals from injured individuals in complex and volatile field environments is of critical importance [1]. Physiological electrical signals can reflect multiple physiological parameters and states of the human body [2,3]. Taking electrocardiographic (ECG) signals as an example, after being captured by electrodes and processed, medical personnel can assess the physical condition of the injured person based on abnormal heart signals and determine the rescue strategy [4,5]. However, at accident scenes, injuries such as abrasions, crush wounds, and burns often result in large open wounds, dust, and bloodstains on the skin, posing significant challenges to signal acquisition [6]. Although conventional patch electrodes play a key role in daily health monitoring and medical applications, their limitations become pronounced in emergency rescue scenarios. In the presence of dust, hair, bloody wounds on the skin, as well as external moisture, sweat, or even blood, these electrodes often exhibit reduced adhesiveness to the skin, leading to electrode dislodgement and signal distortion [7,8]. Moreover, their inadequate breathability can cause skin discomfort during prolonged wear, and may even induce inflammation, swelling, and itching [9].

To address these issues, various improvements have been explored, such as thinning electrodes to enhance

conformability and adhesion [10], developing three-dimensional needle-like electrodes with protrusions to mitigate the effects of dust and liquids [11], or experimenting with flowable materials [12]. However, these approaches often involve complex fabrication, risk of secondary injury, potential infection, or insufficient adhesion, rendering them unsuitable for disaster rescue operations. In this context, fiber-based sensing has garnered attention [13,14]. Novel materials such as composite nanofibers [15], graphene-based conductive fibers [16], and polyurethane yarns [17] have been utilized to develop highly sensitive, flexible, and biocompatible sensors. At present, conductive fibers can be woven into wearable textiles that ensure comfortable fit while enabling real-time monitoring of physiological signals such as heart rate and blood pressure [18].

In recent years, room-temperature liquid metals based on low-melting-point gallium have demonstrated unique advantages in the field of flexible electronics [19-21], owing to their high fluidity at room temperature [22], high electrical conductivity [23], solid–liquid phase transition behavior [24], and good biosafety [25]. Compared to strategies such as rigid metal structures, conductive nanoparticle doping, and ionic flexible conductors, liquid metal-based flexible conductive materials combine high deformability, high conductivity, and ease of fabrication. These gallium-based alloys, merging the advantages of metals and liquids, have achieved significant results in the multifunctional integration of flexible electronics, as well as in biomedical health monitoring and wearable devices [26-28]. Due to their excellent electrical conductivity, low-melting-point phase transition, good fluidity, adhesion, and high biosafety, liquid metals have become an ideal choice for manufacturing flexible conductive fibers and have shown great potential in biomedical sensing [29,30]. For instance, Lin et al. fabricated liquid metal fibers by infusing liquid metal into silicone tubes and secured them onto garments using a digital embroidery method, resulting in fibers with superior electrical and mechanical properties [31]. Lee et al. created wearable circuits by integrating conductive fibers with electronic components and sewing them into fabrics [32]. The mechanical strength of these fibers and their suitability for large-scale coating make it feasible to incorporate them into commercial textiles using standard sewing machines [33]. Chen et al. developed an innovative liquid metal fiber-based iontronic sensor by crossing two hollow porous ionogel fibers to construct pressure and temperature sensors [34].

In view of the limitations of traditional patch electrodes in emergency disaster rescue scenarios, where environmental conditions and skin state often hinder stable ECG signal acquisition, this study proposes a breathable, highly robust surface electrode based on semi-liquid metal (SLM) fibers. The electrode employs elastic fibers as the substrate, which are pre-stretched to impart wrapping constriction force, combined with SLM to achieve high conductivity. The flexibility and conformability of the SLM fiber electrode overcome the interference from factors such as hair, oil, dust, and dirt on the skin of the injured in emergency rescue scenarios, enabling stable ECG acquisition even under adverse skin conditions. In addition, the highly breathable structure of the SLM fiber electrode enables long-term and comfortable non-invasive ECG monitoring after surgery. This innovation expands the applicable population and scenarios for ECG monitoring, offering the potential for comprehensive and accurate health protection.

Results

Design concept and structure of the SLM fiber electrode

To address the limitations of patch electrodes in emergency disaster rescue scenarios, we propose an innovative strategy utilizing elastic conductive fibers wrapped around limbs for ECG monitoring. Here, the contraction force of pre-stretched elastic fibers replaces the adhesive force of conventional patches. During wrapping, the continuous contraction force acts on the skin, forming a mechanical "anchoring" effect that enhances attachment. The wrapped fiber structure can push aside body hair and dust, ensuring electrical contact through mechanical conformity. The flexibility of the elastic fibers allows adaptation to arbitrary limb curvatures, maintaining continuous skin contact during skin deformation and limb movement, thereby ensuring signal acquisition stability. The parallel fiber arrangement enhances electrode breathability, improving comfort during prolonged monitoring. The elastic fiber electrodes can be deployed through a two-step process of "wrapping and securing" in 30 seconds. This electrode fixation method is more

convenient compared with patch electrodes, which require skin cleaning, patch application, and waiting for adhesive stabilization. The poor skin condition and complex patient positions of the injured at disaster rescue sites, the fiber electrode flexibly conforms to limb curvatures, enabling rapid ECG monitoring deployment, as illustrated in **Fig. 1A**. Furthermore, to address the trade-off between high conductivity and high stretchability in conventional conductive fibers, we developed a highly stretchable and conductive SLM based fiber electrode by coating an elastic polyurethane (PU) fiber substrate with the SLM that possesses both high electrical conductivity and high stretchability. However, it was observed that the adhesion between the SLM and the bare fiber was insufficient. To address this, a layer of propylene glycol monomethyl ether acetate (PMA) adhesive was pre-coated onto the PU fiber surface to achieve stable adhesion of the SLM coating, as shown in **Fig. 1B**. In the experiment, simply fully immersing the fibers in PMA glue is sufficient to form a PMA coating on the fiber surface, and strict control of the immersion time and coating thickness is not required. Previous studies [35, 36] have confirmed that abundant hydrogen bonding interactions occur between the PMA adhesive and the metal oxide layer on the SLM surface, resulting in strong interfacial adhesion, as depicted in **Fig. 1C**.

Due to the high fluidity of liquid metal (EGaIn), which makes it difficult to adhere stably to the fiber surface, we reduced its fluidity by incorporating solid metal particles, thus producing the SLM, as shown in **Fig. S1**. Previous studies often used copper particles as dopants to reduce the fluidity of EGaIn [37]. However, the poor wettability between copper particles and the EGaIn led to inhomogeneous dispersion. Based on previous studies indicating that silver exhibits better wettability with EGaIn than copper [38], we used silver-coated copper particles as the dopant for SLM fabrication. Sodium hydroxide (NaOH) solution was used to remove the oxide layer on the EGaIn surface, thereby improving the wetting of silver-plated copper particles by the EGaIn. In addition, as the doping ratio of solid metal particles increases, its electrical conductivity progressively improves (**Fig. S2**), reaching a maximum of 9×10^6 S/m at a doping ratio of 15%, due to the stability and higher electrical conductivity of silver-plated copper particles. However, when the doping ratio exceeds 20%, the SLM loses its fluidity, and at 25% doping, it fails to form a continuous bulk material, as shown in **Fig. S3**. To achieve relatively high electrical conductivity while ensuring the SLM can deform concomitantly with the PU fiber during stretching, a doping ratio of 15% was selected for fabricating the fiber electrodes. As illustrated in **Fig. S4**, the SLM adheres stably to the adhesive panel and retains its morphology without gravity-induced deformation. In contrast, the EGaIn is unable to maintain stable adhesion to the panel and deforms under gravity. Moreover, SEM images in **Fig. S5** further demonstrate that no significant morphological changes were observed on the SLM surface, and no solid metal particles separated from the SLM matrix even after one months of storage. These results demonstrate that the SLM maintains long-term structural stability on the fiber surface, meeting the requirements for long-term use and storage. The X-ray Photoelectron Spectroscopy (XPS) curves in **Fig. S6** indicate that the surface of the SLM is encapsulated by a metal oxide film predominantly composed of gallium oxide, which effectively prevent oxidation by air. The fabrication process of the SLM fiber is illustrated in **Fig. S7**.

Furthermore, to further increase the amount of SLM coated on the PU fiber surface, we designed a double-helical structured PU fiber core. Geometric models were established for the cross-sections of single-strand SLM fibers, double-strand parallel SLM fibers, and double-helical SLM fibers, and the effective areas of the SLM coating in these three structural configurations were calculated, as shown in **Fig. 1D**. Equations (1) to (3) represent the cross-sectional areas of the SLM coating for the single-strand, double-strand parallel, and double-helical SLM fibers, respectively:

$$S_1 = \pi d^2 + 2\pi rd \qquad (1)$$

$$S_2 = \pi d^2 + (2\pi + 4)rd + (4 - \pi)r^2 \qquad (2)$$

$$S_3 = \pi(2r + d)^2 - \frac{2\pi r^2}{\cos\alpha} \qquad (3)$$

Herein, d denotes the thickness of the SLM coating on a single fiber, which is 35 μm; r represents the radius of a single fiber, which is 200 μm, and α is the helical angle, which is 20°. Through calculation of the cross-sectional areas of the SLM coating for the three types of SLM fibers, it was found that the cross-sectional

area of the SLM coating on the double-strand helical SLM fiber is 0.1066 mm², while those of the single-strand and double-strand parallel SLM fibers are 0.0258 mm² and 0.0484 mm², respectively. It can be found that the cross-sectional area of the SLM coating on the double-strand helical SLM fiber is 413% and 220% larger than that of the single-strand and double-strand parallel SLM fibers, respectively. Moreover, the micrograph in **Fig. 1D** visually demonstrates a greater amount of SLM coated on the surface of the double-helical SLM fiber. To quantify this, we fabricated SLM fibers of varying lengths with the three different configurations and measured the mass of the SLM coating on each, as shown in **Fig. S8**. The results demonstrate an average SLM loading capacity of 7 mg/cm for the double-helical fiber, significantly exceeding the values of 2 mg/cm and 5 mg/cm recorded for the single-strand and double-strand parallel configurations, respectively. The SLM loaded on the double-helical fiber is 76% lower than the theoretical value. This significant reduction may be attributed to the uneven distribution of SLM across various parts of the fiber. As visible in **Fig. 1E**, the SLM coating not only provides enhanced electrical conductivity but also deforms under the fiber's contraction force when wrapped onto the skin, conforming closely to skin wrinkles. Besides, the double-helical SLM fiber, with its greater SLM loading, establishes a larger contact area with the skin, and thereby improving signal quality. The skin-electrode contact impedance of three SLM fiber structures was measured at 60 Hz. Results showed that the double-helical SLM fiber had an impedance of 2.3×10^5 Ω, which was substantially lower than that of the single-strand SLM fiber (5.9×10^5 Ω) and double-strand parallel SLM fiber (3.6×10^5 Ω), as illustrated in **Fig. S9**.

Mechanical and electrical properties, and microstructural characterization of SLM fibers

For flexible electrodes, stretchability and flexibility are essential fundamental properties. Accordingly, we fabricated five distinct structural configurations of SLM fibers: single-strand fiber, double-strand parallel fiber, triple-strand parallel fiber, double-helical fiber, and triple-strand braided fiber, and conducted detailed characterization of their mechanical properties, as shown in **Fig. 2A**. The results revealed that the double-helical SLM fiber exhibited the highest elongation at break, reaching 570%, significantly exceeding the 350% elongation of the single-strand fiber. Furthermore, we evaluated the relative resistance change (R/R_0, where R is the resistance under strain and R_0 is the initial resistance) of these five structural types under 100% (**Fig. 2B**) and 200% (**Fig. S10A**) strains over 20 stretching cycles to assess the reproducibility of electrical response. The inset in **Fig. 2B** illustrates the PU fiber cores of all five structures. The time-dependent R/R_0 curves (relative to stretching progression) indicate that the single-strand fiber showed large fluctuations and an overall increasing trend in relative resistance, reflecting poor electrical stability during deformation. When subjected to force, the single-strand fiber experiences localized strain concentration, leading to structural destruction of the SLM coating and consequent significant resistance variation. The double-strand parallel fiber exhibited improved stability compared to the single-strand fiber, though considerable resistance fluctuations remained. The resistance variability of the single-strand fiber and the double-strand parallel fiber during 500 cyclic stretches in **Fig. S10B** also indicates that multi-strand fibers can maintain better electrical stability. The limited mechanical synergy between the two parallel strands resulted in uneven stress distribution during stretching, adversely affecting electrical stability. The triple-strand parallel fiber showed further reduced fluctuation in R/R_0, yet still underperformed relative to helical configurations. Although increasing the number of parallel strands partially enhances structural stability, issues such as inter-fiber sliding in parallel arrangements continue to cause resistance instability. The double-helical fiber demonstrated a relatively stable R/R_0 curve with minimal fluctuation. The helical architecture facilitates stress distribution through its spiral morphology, promoting uniform deformation within the SLM coating and thus stable electrical performance. The triple-strand braided fiber exhibited slightly greater resistance variability than the double-helical structure, likely because its complex triple-strand structure introduces increased inter-fiber interactions when strained, leading to localized stress concentrations that compromise consistent electrical behavior. Overall, the double-helical fiber structure displayed the smallest fluctuation in R/R_0 over 20 cycles at 100% and 200% strain, indicating the most stable electromechanical performance. Not only loading more SLM, but Its helical morphology effectively distributes tensile stress, enabling uniform deformation of the internal SLM coating and ensuring consistent electrical output. This makes it particularly suitable for flexible electrodes requiring long-term mechanical and electrical stability. Therefore, the double-helical fiber was selected for subsequent fabrication of fiber

electrodes in this study. SEM images in **Fig. 2C** confirm that the PU fiber serves as the mechanical substrate, the PMA coating acts as an interfacial mediator, and the SLM coating provides conductive functionality. The SLM coating uniformly envelops the substrate, forming a continuous conductive layer. Adhesion comparison tests in **Fig. 2D** further demonstrate that pre-coating the PU fiber with PMA significantly enhances the adhesion of the SLM coating from 0 kPa to 2.4 kPa, effectively addressing the poor intrinsic adhesion between SLM and PU fiber. Previous studies have demonstrated that the high adhesion provided by the PMA coating can overcome the influence of gravity [24], firmly immobilize SLM on the fiber surface, and sufficiently meet the requirements for daily use [35].

The stretch-release testing results of the SLM fiber demonstrate that during the stretching phase (0% to 200% strain), the fiber morphology extended uniformly without fracture or cracking of the conductive layer. During the release phase, the fiber recovered its original morphology, as shown in **Fig. 2E** and **Video S1**. Micrographs provided in **Fig. S11** further confirm that the oxide film on the SLM surface ruptures during stretching, allowing the encapsulated liquid metal to flow and thereby ensuring stable electrical conductivity. These results indicate that the SLM fiber exhibits excellent deformation adaptability, which is attributed to the synergy between the fluidic properties of the SLM and the elasticity of the PU fiber substrate. During stretching, the SLM coating deforms flexibly with the substrate, avoiding brittle fracture. Upon release, the substrate's elasticity facilitates shape recovery, maintaining the continuity of the conductive layer and ensuring electrical stability under dynamic mechanical conditions. Compared with other reported conductive materials (Materials 1–8, see **Table S1** for details), the SLM exhibits a high electrical conductivity on the order of 10^7 S/m (**Fig. 2F**), significantly surpassing most conventional conductive materials. This outstanding electrical performance stems from the intrinsic high conductivity of the SLM and its uniform, continuous bulk structure, which collectively reduce signal transmission loss in flexible electrodes.

In surface ECG monitoring, stable adhesion between the electrode and the skin is crucial for signal acquisition quality. Conventional patch-type electrodes rely on adhesive strength and are susceptible to influences from skin condition and physical activity. In contrast, SLM fiber electrodes, due to their unique physical morphology, can establish robust mechanical fixation on the skin through wrapping methods, offering distinct advantages. Herein, we developed three fixation methods for SLM fiber electrodes, including knotting (KNT), overlapping (OVL), and adhesion (ADH), while conventional silver/silver chloride (Ag/AgCl) patch electrodes were selected as controls. The SLM fiber electrodes were wrapped around the finger, and the patch electrodes were attached conventionally. The peeling forces of the three fixation methods under normal skin conditions were tested, and the peeling force (N/cm) were recorded and statistically analyzed, as shown in **Fig. 3A**. The peeling force of the SLM fiber electrodes varied among the different fixation methods (the numbers following the fixation methods indicate the number of wrapping turns). In the KNT group, KNT3 exhibited significantly higher peeling force than KNT1 and KNT2, reaching 9.2 N/cm. In the OVL group, OVL3 demonstrated outstanding fixation strength, reaching 5.8 N/cm. The ADH group overall showed relatively lower peeling force. Thus, it can be concluded that as the number of fibers wrapping turns increases, all three fixation methods exhibit higher peeling force. Compared to the conventional patch electrode, which had a peeling force of only 1.3 N/cm, most fixation methods (KNT3 and OVL3) demonstrated superior fixation strength, indicating that the mechanical wrapping approach of SLM fiber electrodes outperforms the adhesive mode of conventional patches in establishing robust fixation. This difference arises because wrapped fixation utilizes mechanical interlocking, whereas conventional patches depend on the adhesion of viscous materials to the skin. Mechanical wrapping is more stable and less affected by skin surface oils, keratin, and other factors. Furthermore, the peeling force of SLM fiber electrodes with the KNT3 fixation method and conventional patch electrodes was measured under simulated challenging skin conditions (contaminated with hair, water, oil, mud, and dust), as shown in **Fig. 3B**. In these simulated challenging interface tests, the conventional Ag/AgCl patch electrode lost its adhesion to the skin, with peeling force dropping to 0 N/cm. In contrast, the SLM fiber electrode maintained peeling force ranging between 7.3–9.1 N/cm, consistently far exceeding that of the conventional patch electrode. This is because the adhesion of conventional patch electrodes relies on interface cleanliness and viscosity, which are compromised in harsh environments. In contrast, the

fixation of SLM fiber electrodes operates through physical wrapping forces, which are less affected by skin surface contaminants, enabling sustained stable attachment. To evaluate more comprehensively the peeling force advantage of SLM fiber electrodes, we included data from 11 other patch-type electrode materials (Materials 1–11, see **Table S2** for details) reported in the literature for comparison. As shown in **Fig. 3C**, the peeling forces of these 11 conventional patch-type electrode materials were generally low, mostly in the range of 0–3 N/cm. Among them, only Material 3 (silk protein/calcium ions/silver nanoparticles) showed a relatively prominent peeling force of approximately 3 N/cm, which was still considerably lower than that of the SLM fiber electrode (9 N/cm). This further confirms that the wrapped fixation of SLM fiber electrodes establishes stronger interfacial bonding than the adhesive mechanism of conventional patch-type electrodes, ensuring electrode-skin interface stability during ECG monitoring and providing reliable ECG signal acquisition in complex environments.

Wearable electrodes require breathability to facilitate gas exchange with the environment, which is crucial for improving wearing comfort. Herein, we evaluated the breathability of 13 groups of SLM fibers through water loss tests and compared them with several commonly used breathable patch electrode materials, including commercial ECG electrode patches, electrospun breathable membrane (ESM), cotton cloth (CC), and medical adhesive tape (MAT). As shown in **Fig. 3D**, multiple SLM fibers were aligned in parallel over a water-containing vessel to form arrays with different fiber spacings, thereby allowing comparison of breathability across varying arrangement densities (**Fig. S12**). The opening of the water container with a width d of 16 mm. The number of fibers N ranged from 6 to 36, defining the fiber spacing as d/N. Therefore, F-6 denotes placing 6 fibers on the water container, and so on; F-36 denotes placing 36 fibers on the water container. The results in **Fig. 3E** show that although the 13 groups of SLM fibers showed no significant differences in moisture loss, they all exhibited significantly higher water loss than conventional breathable patch electrode materials, approaching the level of an open system. Therefore, SLM fiber arrays attached via wrapping provide superior breathability compared to traditional patch electrodes.

Biocompatibility is crucial for long-term health monitoring; therefore, we evaluated the skin compatibility and cell viability of the SLM fiber. Three samples (PU fiber, PMA glue, and SLM) were individually co-cultured with cells in the form of their extracts. Fluorescence live/dead staining images revealed regular cell morphology and minimal numbers of dead cells in both the blank control group and the three sample groups (**Fig. 3F**). Moreover, comparative cell viability results in **Fig. 3G** indicated that none of the three materials exerted significant effects on cell survival, demonstrating that each constituent material of the SLM fiber is non-cytotoxic. Additionally, a small amount of residual SLM from the fiber coating was observed on the skin surface during experiments; however, it could be completely removed using an alcohol wipe, thus preventing potential skin contamination in patients (**Fig. 3H and Video S2**). Finally, the SLM fiber was immersed in a NaOH solution to remove its surface SLM coating. The SLM gradually coalesced and fused into integrated droplets within the NaOH solution (**Fig. 3I** and **Video S3**). The coalesced SLM droplets can be recollected and reused, achieving a recovery rate of 97.6%, which significantly reduces the operational cost of SLM fibers and minimizes material waste, as shown in **Fig. 3J**.

Electrical characterization of the double-helical SLM fibers

Fig. 4A presents the resistance change of an SLM fiber during uniaxial stretching to 180% strain. The inset visually demonstrates the macroscopic morphology of the SLM fiber before and after stretching. Electrical testing employed SLM fiber samples with copper wires bundled at both ends for connection to the resistance measurement instrument. A specific bundling method ensured stable connectivity between the SLM fiber and copper wires, maintaining conduction even at maximum strain, as shown in **Fig. S13**. Here, the initial resistance (R_0) of the 1.8 cm long SLM fiber samples is 0.54 Ω. As depicted in **Fig. 4A**, the SLM fiber was sequentially stretched to various strain levels, each held for 5 s. The results show a gradual increase in resistance, remaining stable at each strain state. Although the SLM fiber exhibited significant resistance change (R/R_0 rising to 4.2 at 180% strain) within the 0–180% strain range, it retained continuous conductivity. Furthermore, the resistance change displayed nonlinear characteristics: relatively gentle at low strains, followed by a pronounced increase at higher strains, suggesting dynamic reconstruction of the SLM coating during stretching. Considering that the stretch rate of human skin during daily physiological

activities ranges from 5% to 45%, and can reach 100% with the assistance of specific devices [39,40], within this range, the SLM fiber's R/R_0 ratio increased only to 2.0, minimally impacting its conductivity. Additionally, the SLM fiber was stretched to 100% strain at different rates (3.6 mm/s, 7.2 mm/s, and 14.4 mm/s), with resistances recorded (**Fig. 4B**). The results demonstrated that the R/R_0 value remained remarkably stable and exhibited consistent periodic variations regardless of the stretching rate. This behavior indicates the reversible electrical response of the SLM fiber under cyclic mechanical stimulation. Cyclic stretching tests (**Fig. 4C**) confirmed the SLM fiber's stable operation at 30%, 60%, 90%, 120%, 150%, and 180% strain, with R/R_0 exhibiting periodic fluctuations, confirming its reliability across deformation amplitudes.

Tests on the influence of humidity variation (**Fig. 4D**) and temperature variation (**Fig. 4E**) on the resistance of SLM fibers showed that the R/R_0 of SLM fibers remained within 0.98–1 across a relative humidity range of 40%–99%, and within 1–1.03 across a temperature range of 15–45 °C. This demonstrates the insensitivity of SLM fibers to environmental temperature and humidity variations, indicating excellent environmental adaptability suitable for physiological environments on the body surface. Furthermore, the SLM fiber was stretched to 100% strain and subjected to 10,000 cycles (**Fig. 4F**). Results indicate that R/R_0 consistently remained within 2.0–2.57 without failure, demonstrating exceptional cyclic stability for long-term dynamic applications. Subsequently, an SLM fiber was wrapped around a volunteer's finger and progressively tightened to increase pressure to 100 kPa, with relative resistance changes recorded during the process, as shown in **Fig. 4G**. R/R_0 increased gradually to 1.18 with rising pressure without substantial change, maintaining continuous conduction. Consequently, the wrapping tightness of the SLM fiber electrode does not compromise its conductive performance, facilitating rapid deployment on the body in practical applications. Subsequently, SLM fibers wrapped around the index finger were compressed by finger pressing to simulate touch interference scenarios encountered in daily life, as shown in **Fig. 4H**. During repeated pressing with an average force of approximately 1.5 N, the R/R_0 of the SLM fibers remained below 0.02, and no visible macroscopic deformation was observed on the skin. Through 14-day long-term resistance monitoring (**Fig. 4I**), the R/R_0 of the SLM fibers increased only to 1.18 without significant fluctuations, demonstrating the stability of the electrical performance of the material system during prolonged service periods and ensuring suitability for long-term wearable applications.

Owing to the unique composite structure and high elasticity of the SLM fibers, conformal contact with the skin was achieved. Compared to conventional Ag/AgCl electrodes, the SLM fibers exhibited superior interface contact, effectively reducing signal transmission impedance and ensuring stable electrical performance. Impedance testing under identical contact areas (**Fig. 4J**) revealed that the SLM fiber electrode exhibited significantly lower impedance than the Ag/AgCl electrode across the frequency range of 0.1–100 kHz. Its impedance measured approximately 0.73 MΩ at low frequency (1 Hz) and decreased to 71 kΩ at high frequency (1000 Hz), indicating superior signal conduction capability. **Fig. S14** presents the interface impedance phase diagram of the SLM fiber electrode, which exhibits similar behavior to the Ag/AgCl electrode. Furthermore, interfacial contact impedance tests at the skin interface for the SLM fiber and Ag/AgCl electrode respectively under five conditions (hair, water, oil, dust, and mud) demonstrate consistently lower impedance for the SLM fiber, as presented in **Fig. S15**. Particularly on dust-covered skin, the SLM fiber conformally adhered to the skin, circumventing dust particles and embedding into skin wrinkles, thereby significantly reducing interface impedance. In contrast, dust interference prevented stable adhesion of the Ag/AgCl electrode to the skin, leading to markedly increased interface impedance. Finally, we measured the skin-electrode interfacial impedance of the fiber electrodes after 1 minute, 10 minutes, and 1 hour of wearing (**Fig. S16**), and the results showed that the skin-electrode interfacial impedance of the fiber electrodes did not change significantly. In summary, the SLM fiber demonstrates outstanding electrical performance in large-strain response, cycling stability, long-term service, temperature adaptation, and physiological signal acquisition.

Unlike bulky ECG devices with commercial rigid wired connections, the ECG monitoring circuit (**Fig. S17**) paired with the SLM fiber electrode features a wireless and portable design, enabling non-invasive, continuous, and real-time monitoring of cardiac health, as shown in **Fig. 5A**. SLM fiber electrodes, wrapped

around a volunteer's index fingers, successfully acquired ECG waveforms that were consistent with those simultaneously recorded by Ag/AgCl electrodes. The magnified local waveforms demonstrate that the SLM fiber electrode captures the ECG waveforms with comparable accuracy to the Ag/AgCl electrode, clearly resolving the P wave, QRS complex, and T wave, with minimal baseline drift and external interference (**Fig. 5B**). This indicates that the SLM fiber electrode matches traditional medical electrodes in ECG signal acquisition quality. The rapid wrapping design of the SLM fiber electrode facilitates the quick deployment of ECG monitoring equipment in emergency rescue scenarios. The SLM fiber electrode enables rapid single-handed wrapping (completed within 10 seconds), and its inherent elasticity automatically adjusts tightness to fit patients of varying sizes (from children to adults), ensuring effective electrode-skin contact. Furthermore, The SLM fiber electrode is stretchable (with a functional strain limit of 180%) with body movements. It can stably adhere to the skin surface even when the skin is stretched (**Fig. S18**) and limb movements (**Fig. S19** and **Video S4**), thereby avoiding electrode detachment or signal interruption caused by limb movements. This makes it suitable for monitoring injured individuals during motion, such as during stretcher transfers or helicopter rescues. Notably, traditional ECG monitoring sites on the injured individuals' body are often not readily accessible in many emergency scenarios. Factors such as chest trauma, burns, compression by objects, or confined spaces within ruins can prevent electrode placement at conventional precordial lead locations. The length of the SLM fiber electrode is highly customizable, allowing rapid wrapping around various body parts. Here, one SLM fiber electrode was wrapped around different body locations of a volunteer (fingers, wrist, arm, thigh, knee, ankle), while another was wrapped around the volunteer's index finger, as shown in **Fig. S20**. Results in **Fig. 5C** show that stable ECG waveforms with clearly discernible P waves, QRS complexes, and T waves, along with minimal baseline drift and external interference, were detected at all six body locations. Therefore, when traditional ECG monitoring sites are inaccessible due to trauma or environmental constraints, the SLM fiber electrode, capable of rapid deployment on multiple body parts, offers an alternative monitoring solution for quickly assessing injured individuals' vital signs.

In emergency rescue scenarios, conventional patch electrodes require skin cleansing and adhesion, prolonging emergency response time. In contrast, the SLM fiber electrode integrates flexibility with conductivity, allowing it to conform closely to the contours of the body. This avoids the signal attenuation often caused by skin folds and surface contaminants when using traditional electrode patches. **Video S5** demonstrates SLM fiber electrodes wrapped around a volunteer's hairy finger skin deliberately contaminated with water, oil, dust, and mud to simulate surface contaminants in rescue scenarios, followed by ECG signal acquisition. Throughout signal collection, the SLM fiber on the skin showed no visible macroscopic deformation and maintained close contact with the skin throughout. **Fig. 5D** displays the ECG waveforms showing that the SLM fiber electrode can stably acquire cardiac signals under five adverse skin conditions. Therefore, the SLM fiber electrodes enable ECG monitoring without skin cleansing, reducing rescue time and avoiding secondary injury caused by skin wiping. Additionally, the fiber configuration provides exceptional breathability, supporting prolonged wear. This significantly reduces risks of allergic reactions or pressure ulcers, particularly beneficial for patients with burns and trauma. As shown in **Fig. 5E**, the ECG acquisition system maintained stability during the 40-minute prolonged monitoring session. The heart rate values exhibited dynamic fluctuations in accordance with physiological states, ranging from approximately 60 to 80 beats per minute, accurately reflecting cardiac rhythm variations. The ECG waveforms could be stably acquired across the initial, middle, and final phases of the test. The RR interval scatter plot demonstrated a characteristic fusiform distribution, with data points densely clustered along the 45° diagonal line, indicating regular sinus rhythm and normal cardiac function in the subject (**Fig. 5F**). Additionally, we monitored ECG signals from four volunteers of different genders and age groups under resting conditions (**Fig. S21**), with all signals consistently displaying discernible QRS complexes and other characteristic waveforms. Furthermore, we have measured the ECG signals of a healthy volunteer during walking and in different postures, and the results demonstrate that movement does not affect the function of the ECG electrodes, as shown in **Fig. S22**. These results demonstrate that the SLM fiber electrode precisely acquires ECG characteristics, providing an innovative solution for developing rapid-deployment cardiac monitoring devices in emergency rescue scenarios. The SLM fiber electrodes used in emergency rescue scenarios are disposable products. To address the issues of environmental pollution and resource

waste caused by disposable medical devices, this SLM fiber can be completely recycled using NaOH solution. **Fig. S23** demonstrates the detachment of the fiber electrode from the PU fiber and its fusion into reusable bulk SLM droplets in the NaOH solution. The mass of the recovered SLM droplets was nearly identical to that of the SLM originally used to fabricate the electrodes. Furthermore, removing the SLM fiber electrode from the patient's skin surface requires only cutting the fiber, enabling automatic detachment without skin damage—particularly advantageous for patients with extensive burns or trauma. In contrast, patch electrodes require 6.8 N of peeling force for removal, causing wound traction and secondary injury, as shown in **Fig. S24.**

Here, we demonstrate the utility of this fiber electrode in Intensive Care Unit (ICU) level postoperative cardiac care for surgical patients, as illustrated in **Fig. 6A and B**. Compared with the IntelliVue patient monitor used in the ICU, the SLM fiber electrode wrapped around the finger not only exhibits accuracy comparable to that of the standard monitor (**Fig. 6C**), but also shows superior biocompatibility and comfort without causing skin irritation such as erythema seen with conventional ECG electrodes (**Fig. S25**). We conducted continuous ECG monitoring for 1 hour on 7 patients using the SLM fiber electrodes. During ECG monitoring, we recorded six types of arrhythmias (**Fig. 6D**), including ST-segment elevation myocardial infarction (STEMI), premature ventricular contraction with concomitant ST-segment depression (PVC with STD), premature atrial contraction with concomitant ST-segment depression (PAC with STD), nonsustained ventricular tachycardia (NSVT), atrial fibrillation (AF), and U wave inversion (UWI). Besides, the battery-powered, high-capacity ECG acquisition system with wireless signal transmission enables continuous, ICU-level remote monitoring for up to 24 hours after surgery. In this study, we selected 4 patients who underwent percutaneous coronary intervention (PCI), craniotomy for hematoma evacuation, coronary angiography, and emergency treatment for acute heart failure, respectively, for 24-hour postoperative ECG monitoring. Their ECG waveforms and heart rates were accurately captured, as shown in **Fig. 6E** and **Fig. S26**. Among them, the case presented in **Fig. 6E** is a myocardial infarction patient (post-PCI) who received extracorporeal membrane oxygenation (ECMO) after cardiac arrest. Initially, the patient exhibited an unstable cardiac rhythm; following intervention, rhythm stability showed marked improvement. Subsequent monitoring revealed that AF patterns on the ECG suggested a potential risk of heart failure. These results demonstrate that the fiber electrode enables prolonged ICU-level postoperative monitoring. Compared with conventional clinical ECG monitors, it is not only simple to operate but also improves wearing comfort.

Discussion

The SLM fiber-based ECG electrode developed in this study effectively addresses the core pain points of traditional patch electrodes in emergency rescue and long-term monitoring scenarios through innovative design and material optimization. The SLM fiber electrode uses pre-stretched elastic PU (polyurethane) fibers as the substrate, and achieves high conductivity (up to 9×10^6 S/m) by coating with SLM. Instead of traditional adhesive patches, it adopts wrap-around fixation to form a mechanical "anchoring" effect. Its double-helix structural design increases the SLM-coated cross-sectional area by 600% compared with single-strand fibers, significantly reducing the skin-electrode contact impedance. Meanwhile, the parallel fiber arrangement ensures high breathability, with moisture loss close to that of an open system, which is significantly superior to traditional materials such as commercial ECG patches and electrospun breathable membranes. The electrode exhibits excellent resistance stability (R/R_0 remains around 1.0) within the temperature range of 15-45℃ and humidity range of 40%-99%, and maintains continuous conductivity after 10,000 cyclic stretches, enabling it to adapt to dynamic interferences caused by limb movements and skin deformation. In terms of biocompatibility, the PU fibers, PMA (polymethyl acrylate) adhesive, and SLM are all non-cytotoxic. Residual SLM can be removed by wiping with alcohol, and the recovery rate reaches 97.6% after treatment with NaOH (sodium hydroxide) solution, achieving both safety and environmental friendliness. In terms of practical application effects, the electrode enables reliable ECG monitoring in multiple scenarios. In emergency rescue, deployment can be completed within 30 seconds without skin cleaning; even when the skin is contaminated with hair, oil, mud, etc., it can still maintain a peel strength of 9.2 N/cm through wrapping force (far exceeding the 1.3 N/cm of traditional Ag/AgCl

(silver/silver chloride) patches), stably collecting complete ECG waveforms including P waves, QRS complexes, and T waves. Moreover, it can flexibly wrap around multiple limb parts such as fingers, wrists, and thighs, solving the problem that traditional chest leads cannot be used in scenarios such as chest trauma and burns. In post-operative monitoring, its high breathability supports continuous wearing for more than 40 minutes without skin irritation reactions such as redness and itching. It can realize 24-hour ICU-level remote monitoring through wireless modules, accurately capturing various arrhythmia signals, thus providing a comfortable and accurate monitoring solution for post-operative patients.

However, the SLM fiber electrode still has shortcomings that need to be improved. Firstly, the double-helix fiber structure in the preparation process relies on manual weaving, which makes it difficult to achieve large-scale mass production and restricts its wide application. Besides, in terms of fixation method, although KNT3 has the strongest fixing force, it may cause local compression on patients with burns or large-area trauma. In addition, it is currently only optimized for ECG signals and has not been extended to the monitoring of other physiological electrical signals such as electromyography (EMG) and electroencephalography (EEG), resulting in a single function. Finally, the recovery of SLM requires complete stripping from PU fibers using a NaOH solution, which may damage the PU fibers and reduce their number of reuses. To address the above issues, future optimization can be promoted from the following aspects. Firstly, we will develop automated weaving and coating equipment to realize mass production of double-helix fibers through precise mechanical control, thereby reducing costs and ensuring structural consistency. Besides, design an adaptive fixation system that combines elastic bandages and adjustable buckles to maintain fixation strength while avoiding skin compression, adapting to patients with different trauma types. In addition, expand sensing functions and develop integrated sensors compatible with multiple signals including ECG, EMG, and EEG. Finally, simplify the recovery process and develop degradable fiber cores to realize rapid recovery of SLM fibers in neutral solutions.

Methods

Materials

Gallium (Ga, 99.9%) and indium (In, 99.9%) were procured from Anhui Minor New Materials Co., Ltd. Silver-plated copper microparticles with a mean diameter of 15 μm and an Ag content of 3 wt% were obtained from Hebei Jingrui Alloy Products Co., Ltd. PU fibers (diameter of 200 μm) were acquired from Ningbo Prem Sewing Equipment Co., Ltd. PMA glue was purchased from Dongguan Yihui Adhesive Co., Ltd. A sodium hydroxide solution (1.0 mol L^{-1}) was sourced from Xi Long Science Co., Ltd.

Fabrication of semi-liquid metal (SLM)

First, gallium (75.5 wt%) and indium (24.5 wt%) were mixed in a beaker, followed by heating at 200°C for 2 hours. Subsequently, silver-plated copper microparticles (15 wt%) were added to the resultant liquid metal (EGaIn). An appropriate amount of 1.0 mol L^{-1} aqueous NaOH solution was then poured into the beaker. After 3 minutes of stirring, the silver-plated copper microparticles were dispersed into the liquid metal, yielding the SLM.

Fabrication of SLM fiber

Four types of polyurethane (PU) fiber structures (double-strand parallel fiber, triple-strand parallel fiber, double-helical fiber, and triple-strand braided fiber) were fabricated via manual braiding. Subsequently, single PU fiber and the four structured PU fibers were separately immersed in propylene glycol monomethyl ether acetate (PMA) glue for one minute. Following immersion, the five PU fiber groups were removed from the PMA glue and air-dried under ambient conditions to form PMA films on their surfaces. This step reinforced the multi-fiber assemblies and enhanced adhesion between PU fibers and the SLM through PMA film encapsulation. Finally, SLM was uniformly coated onto all five PU fiber groups using a brush.

Electrical characterization

The electrical conductivity of SLM with varying doping ratios (0, 5, 10, 15, 20 wt%) was measured using the standard four-probe technique. Samples were filled into trapezoidal grooves measuring 50 mm in length

with a cross-sectional area of 15 mm². Both ends of the SLM fibers were bundled to copper wires for connection to testing instruments. SLM fiber samples with different structural configurations were secured on a dynamic mechanical test system (HC-01, Dongtai Suheng Transmission Technology Co., Ltd.), while resistance changes during stretching were monitored with a multimeter (U1251B, Agilent Technologies, Inc.). A four-terminal method was employed to eliminate contact resistance effects. Commercial Ag/AgCl electrodes (X-1, Hangzhou Xunda Wireless Electric Appliance Co., Ltd.) and SLM fibers were attached to the fingers of healthy volunteers (25-year-old female; 31-year-old female; 28-year-old male; 31-year-old male), and skin-electrode impedance was characterized over the frequency range of 0.1–100,000 Hz using an electrochemical workstation (CHI760E, CH Instruments, Inc.). SLM fibers were placed in a constant temperature-humidity chamber (TEMP&HUMI, Shanghai Keken Test Equipment Co., Ltd.) with resistance monitored by a digital multimeter (Keithley 2002, Tektronix Inc.) under varying temperature and humidity conditions.

Mechanical characterization

The stress-strain curves of SLM fiber samples with different structures were measured using a dynamic mechanical test system (HC-01, Dongtai Suheng Transmission Technology Co., Ltd.). The adhesion of the SLM to the PU fiber and its adhesion to the PMA coating were measured using the dynamic mechanical test system. A segment of PU fiber and a segment of PU fiber coated with PMA were separately attached to the bottom of the force gauge. Subsequently, both samples were inserted into the SLM at a speed of 1 mm/s to a depth of 1 mm, followed by an upward pull of 6 mm. The force gauge was used to record the adhesion force between the samples and the SLM during this process. One end of the SLM fiber was fixed to the force gauge, while the other end was attached to a volunteer's finger using three different wrapping methods: knotting (KNT), overlapping (OVL), and adhesion (ADH). The SLM fiber was pulled downward by the force gauge until it detached from the finger, and the tension experienced by the SLM fiber during this process was recorded. Similarly, the SLM fiber was attached to fingers with hair, water, oil, dust, or mud by wrapping it three times and finishing with a KNT (KNT3) method and pulled downward by the force gauge until detachment. The tension on the SLM fiber during this process was recorded. For comparison, an Ag/AgCl electrode patch was attached to a volunteer's finger and pulled downward by the force gauge until it detached from the skin. The adhesion force between the Ag/AgCl electrode patch and the skin during this process was recorded.

Breathability test

The moisture permeability was evaluated based on the weight loss of water from a container (opening area: 16 mm × 16 mm). The test sample was placed over the container containing 10 g of water. The assembly was then placed in a ventilated area for 7 days, after which the remaining water mass was measured.

Morphology characterization

All SEM images were captured using an environmental scanning electron microscope (Apreo, Thermo Fisher Technology Co., Ltd). The surface and cross-section morphology of the PU fiber, PMA coating, and SLM coating was characterized using an optical microscope (FHD Camera V2, Shenzhen Shunhuali Electronics Co., Ltd.). The valence states of elements were characterized by XPS (ESCALAB 250Xi, Thermo Fisher Scientific, Oxford, UK).

Cell experiments

HaCaT cells were cultured in Dulbecco's Modified Eagle Medium supplemented with 10% fetal bovine serum (FBS, Wisent Corp.) and 1% penicillin-streptomycin (PS, Thermo Fisher Scientific Inc.) for 24 h under an atmosphere of 5% CO_2 at 37 °C. PU, PMA, and SLM were added to the cell culture medium, followed by incubation at 37 °C for 12 h. Subsequently, the extracts of the materials were added to the cells in different experimental groups, and incubation was continued in an incubator for 12 h. After the incubation, the cells were washed 1–2 times. Calcein AM and PI were used to stain the cells to distinguish live cells from dead cells. The negative control group was only added with an equal volume of medium. Finally, before taking pictures with a confocal microscope, Hoechst dye was added to stain the cell nuclei for clear

observation of the nuclei during imaging.

Electrocardiogram (ECG) monitoring

A customized ECG acquisition module (BMD101, NeuroSky Electronic Technology Co., Ltd.) was employed to acquire ECG signals. A 3D-printed enclosure was used to house the ECG module, with two shielded wires terminated with copper clips extending from the enclosure for connection to electrodes. During ECG measurement, the SLM fibers were first secured to a volunteer's left and right index fingers using the KNT3 method. Subsequently, the copper clips on the shielded wires were attached to the SLM fibers on the respective index fingers to measure the ECG signal. In the ICU, a IntelliVue patient monitor (MX550, Philips Medizin Systeme Böeblingen GmbH) was used to record the patients' ECG signals as the control group. Simultaneously, the SLM fibers were secured to the patients' index fingers using the KNT3 method, and the ECG monitoring module was employed to acquire data for the test group. The study collected six types of electrocardiograms from different patients, including ST-segment elevation myocardial infarction, premature ventricular contraction with concomitant ST-segment depression, premature atrial contraction with concomitant ST-segment depression, nonsustained ventricular tachycardia, atrial fibrillation, and U wave inversion. All ECG patterns were confirmed by an experienced physician.

Ethics approval

All procedures involving the application of SLM fiber electrodes on volunteer skin adhered to the ethical guidelines approved by Ethics Committee of Tianjin University (Approval No.: TJUE2025-H-S-021). The clinical application of the SLM fiber electrodes adhered to the ethical guidelines of the Ethics Committee of Wenzhou People's Hospital (Approval No.: KY-202504-012). Informed consent was obtained from all participating volunteers. Research involving human research participants is performed in accordance with the Declaration of Helsinki.

References

1. Chen, K., Lu, X., Chen, R. & Liu, J. Wireless wearable biosensor smart physiological monitoring system for risk avoidance and rescue. *Math. Biosci. Eng.* **19**, 1496-1514 (2022).

2. Tian, Q. et al. Hairy-skin-adaptive viscoelastic dry electrodes for long-term electrophysiological monitoring. *Adv. Mater.* **35**, e2211236 (2023).

3. Zhang, B. et al. A three-dimensional liquid diode for soft, integrated permeable electronics. *Nature* **628**, 84-92 (2024).

4. Jinkins, K. R. et al. Thermally switchable, crystallizable oil and silicone composite adhesives for skin-interfaced wearable devices. *Sci. Adv.* **8**, eabo0537 (2022).

5. Michard, F., Bellomo, R. & Taenzer, A. The rise of ward monitoring: opportunities and challenges for critical care specialists. *Intensive Care Med.* **45**, 671-673 (2019).

6. Li, J. et al. High-performance flexible microneedle array as a low-impedance surface biopotential dry electrode for wearable electrophysiological recording and polysomnography. *Nano-Micro Lett.* **14**, 132 (2022).

7. Wang, C. et al. Flexible patch with printable and antibacterial conductive hydrogel electrodes for accelerated wound healing. *Biomaterials* **285**, 121479 (2022).

8. Song, D., Ye, G., Zhao, Y., Zhang, Y., Hou, X. & Liu, N. An all-in-one, bioderived, air-permeable, and sweat-stable MXene epidermal electrode for muscle theranostics. *ACS Nano* **16**, 17168-17178 (2022).

9. Zhuang, Q. et al. An ICU-grade breathable cardiac electronic skin for health, diagnostics, and intraoperative and postoperative monitoring. *Sci. Adv.* **11**, eadu3146(2025).

10. Li, L. et al. Paintable, fast gelation, highly adhesive hydrogels for high-fidelity electrophysiological monitoring wirelessly. *Small* **21**, e2407996 (2025).

11. Bae, W. G., Kim, D., Kwak, M. K., Ha, L., Kang, S. M. & Suh, K. Y. Enhanced skin adhesive patch with modulus-tunable composite micropillars. *Adv. Healthcare Mater.* **2**, 109-113 (2013).

12. Wu, Z. et al. Stable and dynamic multiparameter monitoring on chests using flexible skin patches with self-adhesive electrodes and a synchronous correlation peak extraction algorithm. *Adv. Healthcare Mater.* **12**, e2202629 (2023).

13. Wang, W. et al. Imperceptible augmentation of living systems with organic bioelectronic fibres. *Nat. Electron.* **7**, 586-597 (2024).

14. Yang, Y., Liu, Y. & Yin, R. Fiber/yarn and textile-based piezoresistive pressure sensors. *Adv. Fiber Mater.* **7**, 34-71 (2024).

15. Tang, C. et al. All-metal flexible fiber by continuously assembling nanowires for high electrical conductivity. *Small* **20**, e2405000 (2024).

16. Ryu, K.-H. et al. Boost up the mechanical and electrical property of CNT fibers by governing lyotropic liquid crystalline mesophases with aramid polymers for robust lightweight wiring applications. *Adv. Fiber Mater.* **5**, 514-526 (2022).

17. Shen, Y. et al. PVF composite conductive nanofibers-based organic electrochemical transistors for lactate detection in human sweat. *Chem. Eng. J.* **475**, 146008 (2023).

18. Ma, Z., Huang, Q., Zhou, N., Zhuang, Q., Ng, S.-W. & Zheng, Z. Stretchable and conductive fibers fabricated by a continuous method for wearable devices. *Cell Rep. Phys. Sci.* **4**, 101300 (2023).

19. Cao, J. et al. Ultra-robust stretchable electrode for e-skin: In situ assembly using a nanofiber scaffold and liquid metal to mimic water-to-net interaction. *InfoMat* **4**, e12302 (2022).

20. Zhuang, Q. et al. Liquid-metal-superlyophilic and conductivity-strain-enhancing scaffold for permeable superelastic conductors. *Adv. Funct. Mater.* **31**, 2105587 (2021).

21. Ma, Z. et al. Permeable superelastic liquid-metal fibre mat enables biocompatible and monolithic stretchable electronics. *Nat. Mater.* **20**, 859-868 (2021).

22. Wang, M. et al. Stencil printing of liquid metal upon electrospun nanofibers enables high-performance flexible electronics. *ACS Nano* **15**, 19364-19376 (2021).

23. Shan, X., Feng, W., Guo, M., Wang, X. & Liu, J. Pan-media liquid metal 3D printing. *Innovation* **6**, 100813 (2025).

24. Guo, R., Wang, H., Chen, G., Yuan, B., Zhang, Y. & Liu, J. Smart semiliquid metal fibers with designed mechanical properties for room temperature stimulus response and liquid welding. *Appl. Mater. Today* **20**, 100738 (2020).

25. Wang, C. et al. Liquid metal: a new approach to diagnosis and treatment of cardiovascular diseases. *Adv. Mater.* **37**, e2505540 (2025).

26. Yang, S., Liu, C., Tang, L., Shang, J., Zhang, J. & Jiang, X. Highly adhesive and stretchable epidermal electrode for bimodal recording patch. *ACS Appl. Mater. Interfaces* **16**, 43880-43891 (2024).

27. Li, N. et al. Fingertip-inspired spatially anisotropic inductive liquid metal sensors with ultra-wide range, high linearity and exceptional stability. *Adv. Mater.* **37**, e2419524 (2025).

28. Peng, Y. et al. Permeable, wet-adhesive, and EMI-resistant liquid metal electronic skin for high-fidelity electrophysiological monitoring in sweaty and electromagnetic environments. *Adv. Mater.*, e08041 (2025).

29. Zheng, L., Zhu, M., Wu, B., Li, Z., Sun, S. & Wu, P. Conductance-stable liquid metal sheath-core microfibers for stretchy smart fabrics and self-powered sensing. *Sci. Adv.* **7**, eabg4041 (2021).

30. Yu, X. et al. A one-step fabricated sheath-core stretchable fiber based on liquid metal with superior

electric conductivity for wearable sensors and heaters. *Adv. Mater. Technol.* **7**, 2101618 (2022).

31. Lin, R. et al. Digitally-embroidered liquid metal electronic textiles for wearable wireless systems. *Nat. Commun.* **13**, 2190 (2022).

32. Lee, G. H. et al. Meter-scale heterostructure printing for high-toughness fiber electrodes in intelligent digital apparel. *Nat. Commun.* **16**, 4320 (2025).

33. Wang, H. et al. Liquid metal fibers. *Adv. Fiber Mater.* **4**, 987-1004 (2022).

34. Chen, J., Zhu, G., Wang, J., Chang, X. & Zhu, Y. Multifunctional iontronic sensor based on liquid metal-filled hollow ionogel fibers in detecting pressure, temperature, and proximity. *ACS Appl. Mater. Interfaces* **15**, 7485-7495 (2023).

35. Guo, R., Zhen, Y., Huang, X. & Liu, J. Spatially selective adhesion enabled transfer printing of liquid metal for 3D electronic circuits. *Appl. Mater. Today* **25**, 101236 (2021).

36. Guo, R. et al. One-step liquid metal transfer printing: toward fabrication of flexible electronics on wide range of substrates. *Adv. Mater. Technol.* **3**, 1800265 (2018).

37. Tang, J., Zhao, X., Li, J., Guo, R., Zhou, Y. & Liu, J. Gallium-based liquid metal amalgams: transitional-state metallic mixtures (TransM^{2}ixes) with enhanced and tunable electrical, thermal, and mechanical properties. *ACS Appl. Mater. Interfaces* **9**, 35977-35987 (2017).

38. Xing, Z. et al. Reactive wetting induced instantaneous nanoparticles internalization in gallium-based liquid metal. *Surf. Interfaces* **72**, 107098 (2025).

39. Rupani M, Cleland LD, Saal HP. Local postural changes elicit extensive and diverse skin stretch around joints, on the trunk and the face. *J R Soc Interface.* **22** (223):20240794 (2025).

40. Li WJ, Laurencin CT, Caterson EJ, et al. Electrospun nanofibrous structure: a novel scaffold for tissue engineering. *J. Biomed. Mater. Res.* **60** (4):613–621 (2002).

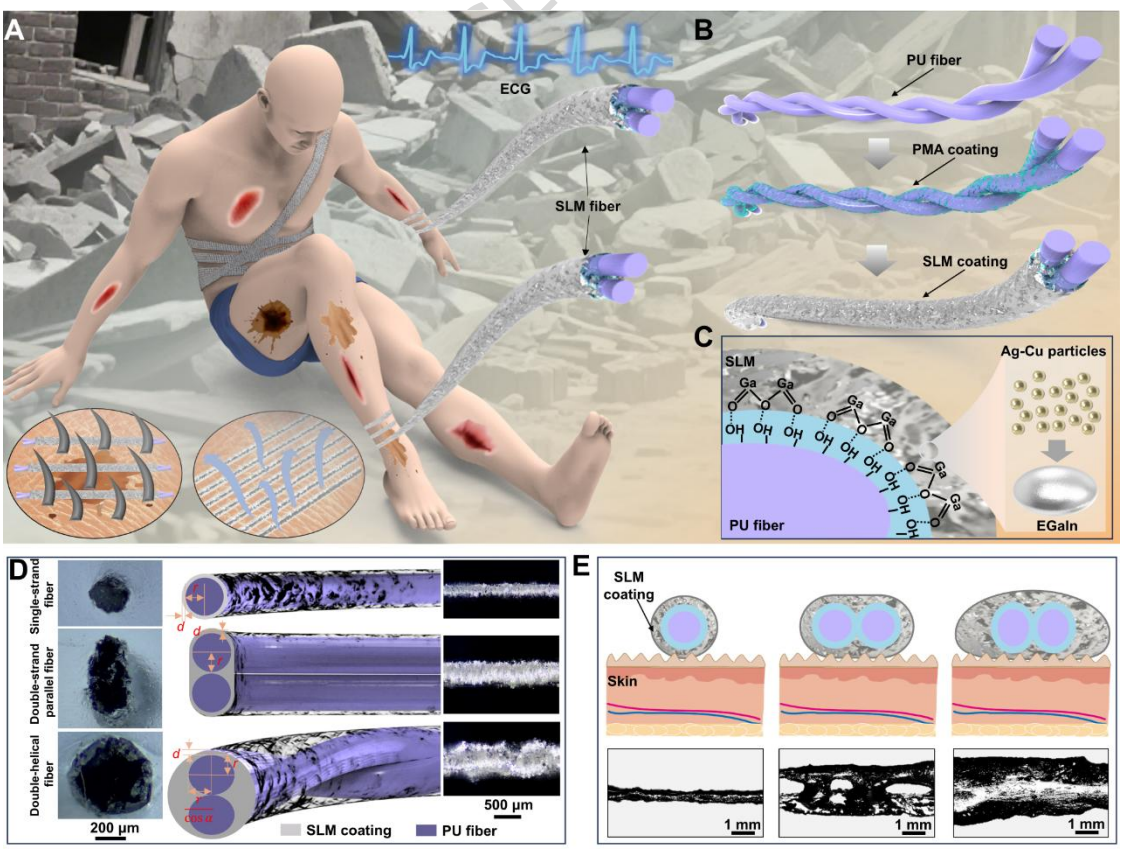

Fig. 1| Schematic of the design concept and structure of the SLM fiber electrode. A Conceptual diagram of SLM fiber electrodes for ECG monitoring in wounded patients. **B** Fabrication process of SLM fiber. **C** Abundant hydrogen bonding interactions between the PMA adhesive and the metal oxide layer on the SLM surface. **D** The cross-sections and of single-strand SLM fiber, double-strand parallel SLM fiber, and double-helical SLM fiber, and their geometric models. **E** Contact area with the skin for single-strand SLM fiber, double-strand parallel SLM fiber, and double-helical SLM fiber.

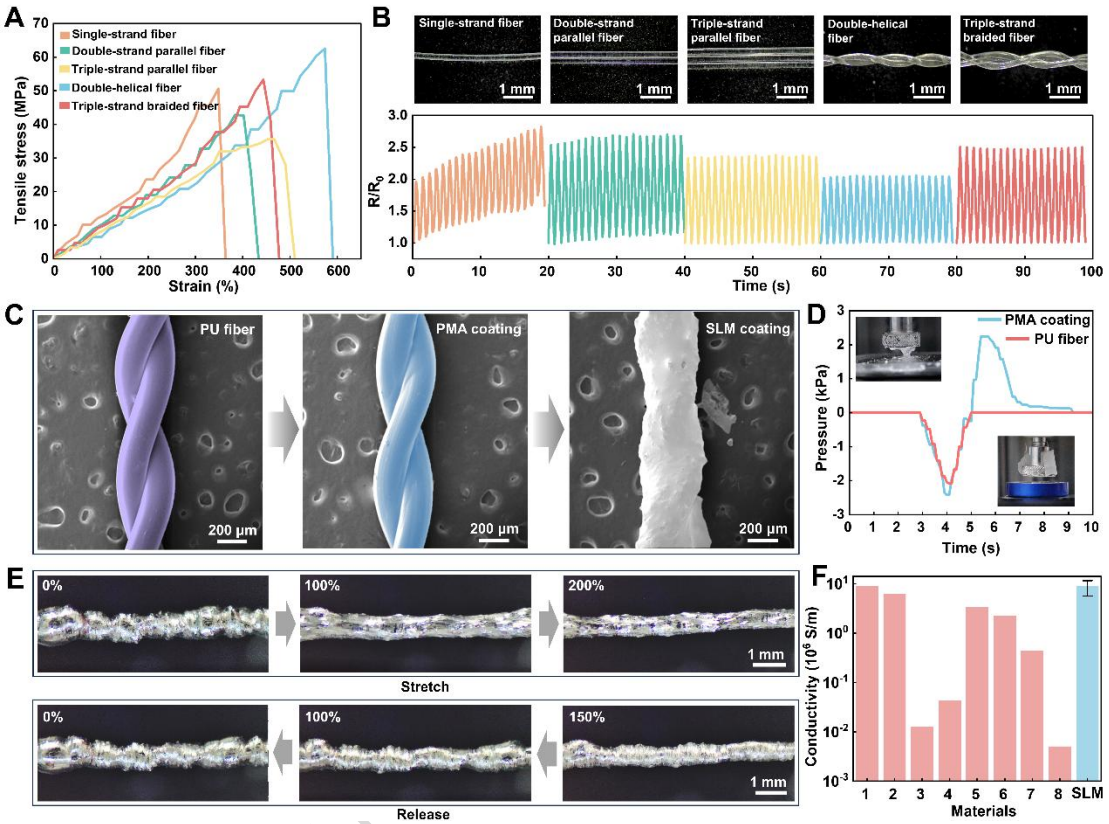

Fig. 2| Comparison of mechanical and electrical properties, and microstructural characterization of SLM fibers. A Stress-strain curves of single-strand fiber, double-strand parallel fiber, triple-strand parallel fiber, double-helical fiber, and triple-strand braided fiber. **B** Relative resistance change of these five structural types under 100% tensile strains over 20 stretching cycles and the PU fiber cores of all five structures. **C** SEM images of PU fiber, PMA coating and SLM coating. **D** Adhesion comparison tests of SLM to PU fiber with and without PMA coating. **E** The stretch-release testing of SLM fiber. **F** Comparison of electrical conductivity between SLM fiber and other reported conductive materials.

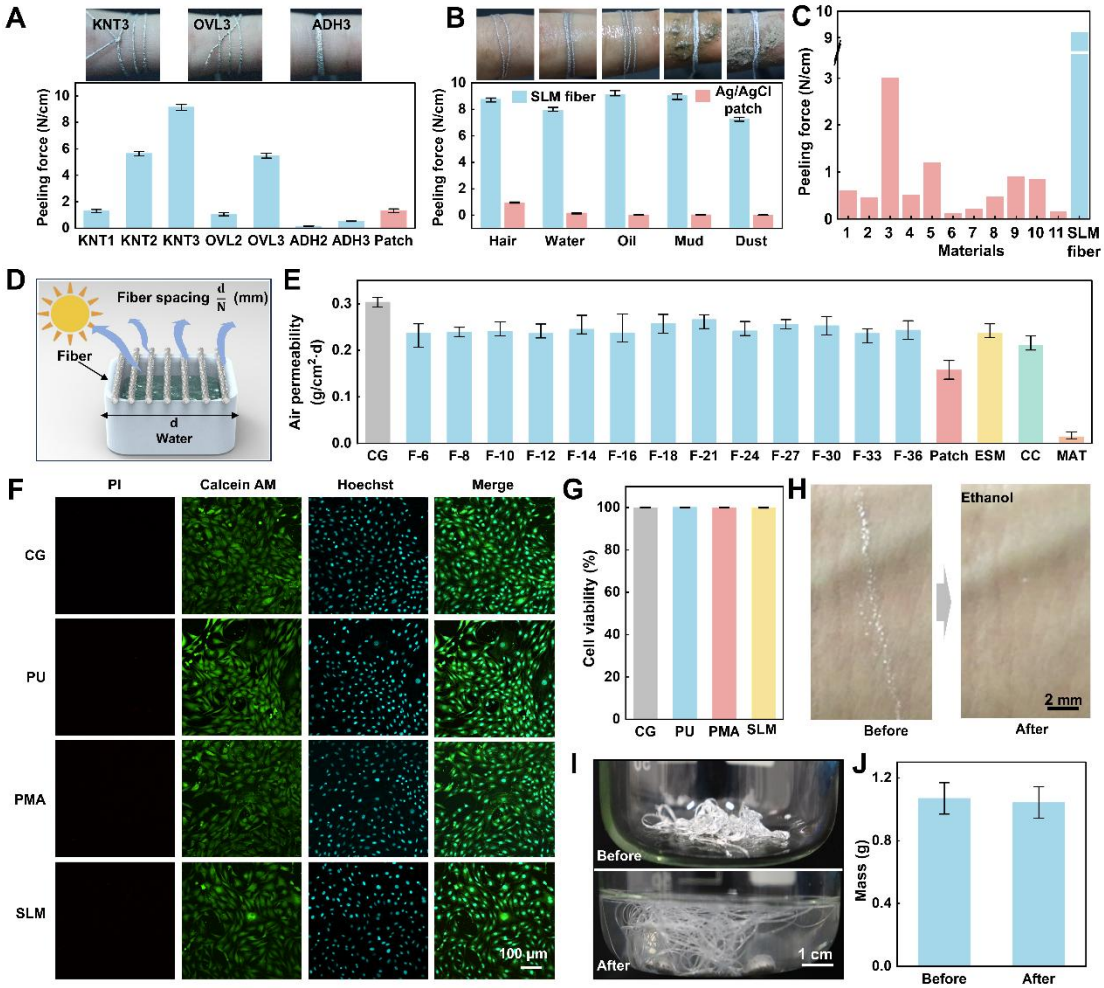

Fig. 3| Evaluation of the skin attachment, breathability, and biocompatibility of the SLM fiber. A Peeling force of SLM fiber electrodes under different fixation methods. **B** Peeling force of SLM fiber electrodes and conventional Ag/AgCl patch electrodes under simulated challenging skin conditions. **C** Comparison of peeling force between SLM fiber and other reported patch-type electrode materials. **D** Arrays of multiple SLM fibers over a water-containing vessel. **E** Air permeability between SLM fiber and other conventional breathable patch electrode materials. **F** Fluorescence live/dead staining images of the blank control group and the three sample groups. **G** Cell viability of the blank control group and the three sample groups. **H** Images before and after removal of SLM residue from skin surface. **I** The fusion of the SLM into integrated droplets within the alkaline solution. **J** Mass comparison of SLM before and after Recycling.

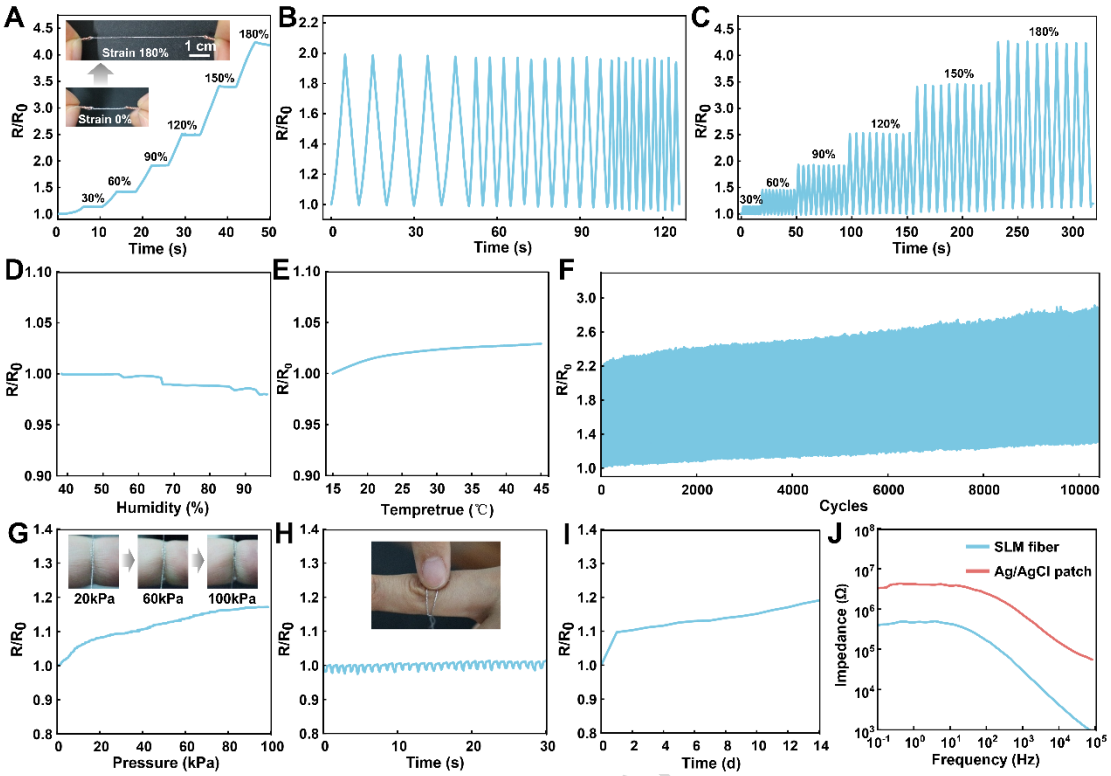

Fig. 4| Electrical characterization of SLM fibers. A Relative resistance change curve of SLM fiber during uniaxial stretching to 180% strain. **B** Relative resistance change curve of SLM fiber at different stretching rates. **C** Relative resistance change curve of SLM fiber under cyclic stretching at various strain levels. **D** Relative resistance change curve of SLM fiber across 40%–99% relative humidity. **E** Relative resistance change curve of SLM fiber within 15–45 °C. **F** Relative resistance change curve of SLM fiber during 10,000 stretching cycles. **G** Relative resistance change curve of SLM fiber under different wrapping pressures. **H** Relative resistance change curve of SLM fiber during repeated pressing. **I** Long-term relative resistance change curve of SLM fiber. **J** Interfacial contact impedance at the skin interface for the SLM fiber and Ag/AgCl electrode.

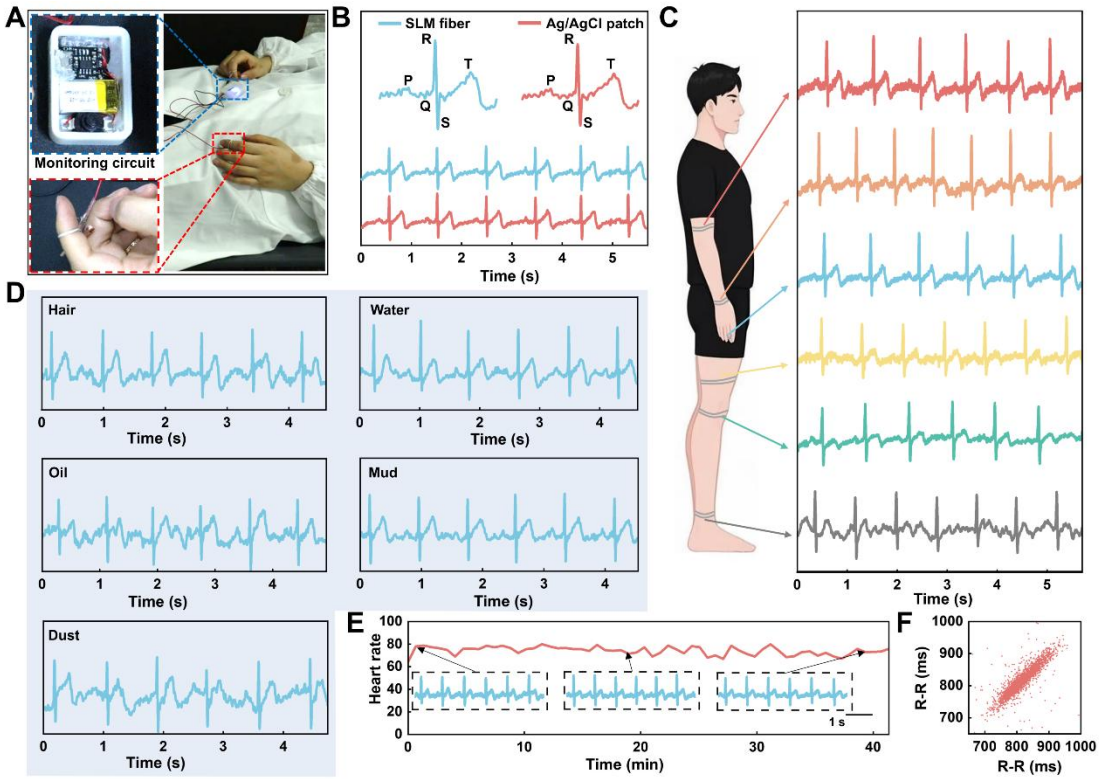

Fig. 5| SLM fiber electrodes for body surface ECG signal monitoring. **A** Photograph of an SLM fiber electrode wrapped around a finger and its paired ECG monitoring circuit. **B** ECG signals simultaneously acquired by the SLM fiber electrode and Ag/AgCl electrode, with magnified waveforms. **C** Six body locations wrapped with SLM fiber electrodes and their corresponding detected ECG waveforms. **D** ECG signals acquired by the SLM fiber electrode under five adverse skin conditions. **E** ECG and heart rate acquired by the SLM fiber electrode during prolonged monitoring. **F** RR interval scatter plot.

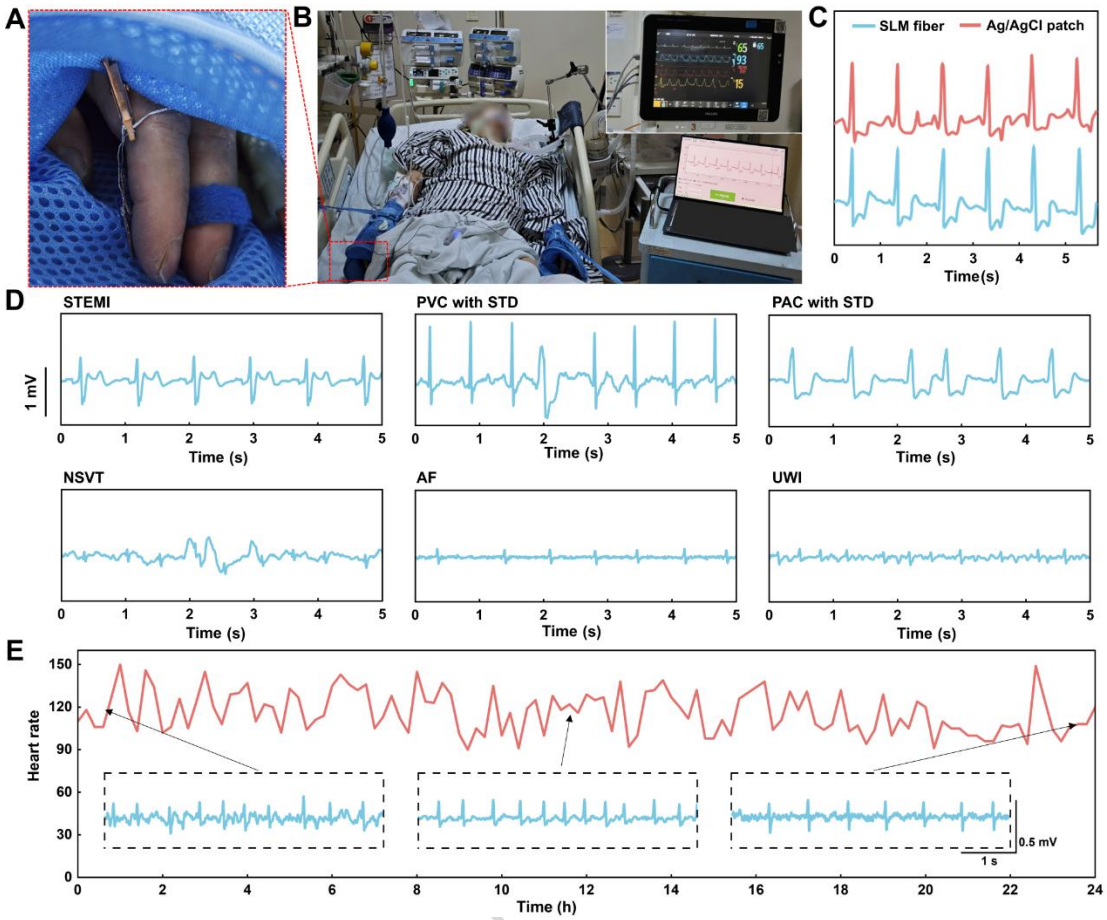

Fig. 6| Continuous postoperative ECG monitoring in ICU patients using the SLM fiber electrode. A SLM fiber electrode wrapped around a patient's finger. **B** Photograph of simultaneous postoperative ECG monitoring using the SLM fiber electrode and a clinical ECG monitor. **C** Comparison of postoperative ECG signals acquired by the SLM fiber electrode and the clinical ECG monitor. **D** Representative ECG waveforms of six types of arrhythmias, including STEMI, PVC with STD, PAC with STD, NSVT, AF, and UWI. **E** Heart rate and ECG waveforms at different time points recorded over 24 hours postoperatively from a patient after PCI using the SLM fiber electrode.

Acknowledgments

This research was supported by the National Natural Science Foundation of China (Grant No. 62304150) and the National Key R&D Program of China (Grant No. 2024YFC3016604)

Author contributions

All authors have read and approved the manuscript. R. G., H. F. and Y. L. conceived and designed the project; X. L. (Xiaotong Liu), H. X., L. C., X. L. (Xin Lyu) and X. W. performed the experiments; X. L. (Xiaotong Liu) and H. X. analysed the data. R. G., X. L. (Xiaotong Liu), H. X., H. F. and Y. L. wrote and revised the article.

Competing interests

The authors declare no competing financial or non-financial interests.

Data and materials availability

The datasets generated and/or analyzed during the current study are not publicly available due to [The dataset is still being used for subsequent related research and has not yet undergone complete collation and validation to ensure its accuracy and integrity.] but are available from the corresponding author on reasonable request.